Tectonophysics 682 (2016) 278–292

Contents lists available at ScienceDirect

Tectonophysics

journal homepage: www.elsevier.com/locate/tecto

Tectonic-geomorphology of the Litang fault system, SE Tibetan Plateau, and implication for regional seismic hazard

Marie-Luce Chevalier [a,*], Philippe Hervé Leloup [b], Anne Replumaz [c,d], Jiawei Pan [a], Dongliang Liu [a], Haibing Li [a], Loraine Gourbet [b,e], Marianne Métois [b]

[a] Key Laboratory of Continental Tectonics and Dynamics, Institute of Geology, Chinese Academy of Geological Sciences, 26 Baiwanzhuang Rd, Beijing 100037, China
[b] Laboratoire de géologie de Lyon, CNRS UMR 5570, Université de Lyon 1, Villeurbanne, France
[c] ISTerre, Université Grenoble Alpes, Grenoble, France
[d] CNRS, ISTerre, Grenoble, France
[e] ETH — Zurich, Geological Institute, Earth Surface Dynamics, Sonneggstrasse 5, 8092 Zurich, Switzerland

ARTICLE INFO

Article history:
Received 20 January 2016
Received in revised form 17 May 2016
Accepted 25 May 2016
Available online 28 May 2016

Keywords:
Litang fault system
Eastern Tibet
Slip-rate
Tectonic-geomorphology
Earthquake hazard
Sichuan

ABSTRACT

The Litang fault system (LTFS) in the eastern Tibetan Plateau has generated several large (7.5 > M > 7) historical earthquakes and has exhumed granitic peaks rising >1700 m above the mean elevation of the plateau, despite being located within a tectonic block surrounded by highly active faults. We study horizontally offset moraine crests from the Cuopu basin and a vertically offset alluvio-glacial fan from the eastern Maoya basin. We determine a left-lateral rate of 0.09 ± 0.02 mm/yr along a slowly slipping secondary fault at Cuopu, while the main active fault at present is the normal range-front N Cuopu fault, along which we determined a left-lateral rate of 2.3 ± 0.6 mm/yr since 173 ka. At Maoya fan, matching the vertical 12 ± 1 m cumulative offset with the 21.7 ± 4.2 ka fan age yields a vertical (normal) rate of 0.6 ± 0.1 mm/yr. This rate is very similar to that recently determined at the same location using low-temperature thermochronology (0.59 ± 0.03 mm/yr since 6.6 ± 0.5 Ma). Left-lateral rates along the main faults of the LTFS range between 0.9 and 2.3 mm/yr at all timescales from a few years to ~6 Ma. The facts that the LTFS is highly segmented and that at present, the Cuopu, Maoya and South Jawa segments are mostly normal (while the Litang and Dewu segments are left-lateral/normal), could prevent the occurrence of M > 7.5 destructive earthquakes along the LTFS, as is generally assumed. However, motion on the normal faults appears to be linked with motion on the strike–slip faults, potentially allowing for exceptional larger earthquakes, and implying that the area is not experiencing pure ~NS extension but rather NW–SE left-lateral transtension.

1. Introduction

Eastern Tibet, while located farther away from the collision front between India and Asia than the Himalayan range, nevertheless displays a major step in the topography, representing the greatest relief on the plateau. The highest peak of the Longmen Shan thrust belt (7556 m, Gongga Shan, 'GS' in Fig. 1B) is adjacent to the ~500 m-high Sichuan basin, over a distance of just ~50 km. This step in the topography more or less marks the boundary between the seismically active Tibetan Plateau (>4000 m a.s.l., >60 km thick crust, numerous active faults) and the tectonically stable plains of eastern China (Ordos basin, Sichuan basin, Fig. 1A, and South China block) (<1000 m a.s.l., <45 km thick crust, fewer active faults). This transition has been referred to as the "NS-trending tectonic zone" or "NS seismic belt" (green box in Fig. 1A) due to the fact that more than one third of all historical M > 7 earthquakes in continental China have occurred in that zone (e.g., Deng et al., 2003; Zhang, 2013), including the devastating 2008 Mw7.9 Wenchuan earthquake. Such great relief related to high seismic activity makes SE Tibet a key region to decipher the different models of the Tibetan Plateau's deformation. While GPS data (Fig. 1B) reveal that eastern Tibet is rotating clockwise relative to Eurasia around the eastern Himalayan syntaxis along the Xianshuihe fault (Zhang et al., 2004; Gan et al., 2007; Liang et al., 2013), what drives this eastward motion is highly debated and may be explained by different mechanisms. While the above GPS studies advocate continuous deformation of eastern Tibet, other studies in contrast, interpreted the same GPS data to show that eastern Tibet is made of blocks separated by active faults (block-like model, Meade, 2007; Thatcher, 2007).

From low temperature thermochronology data, Zhang et al. (2015) showed that vertical motion along the left-lateral/normal Litang fault system (hereafter LTFS), which is parallel to the Xianshuihe fault, initiated between 5 and 7 Ma. They interpreted this age as corresponding

* Corresponding author.
E-mail addresses: mlchevalier@hotmail.com (M.-L. Chevalier), herve.leloup@univ-lyon1.fr (P.H. Leloup), anne.replumaz@ujf-grenoble.fr (A. Replumaz), jiawei-pan@foxmail.com (J. Pan), pillar131@163.com (D. Liu), lihaibing06@163.com (H. Li), loraine.gourbet@ens-lyon.fr (L. Gourbet), marianne.metois@univ-lyon1.fr (M. Métois).

http://dx.doi.org/10.1016/j.tecto.2016.05.039
0040-1951/

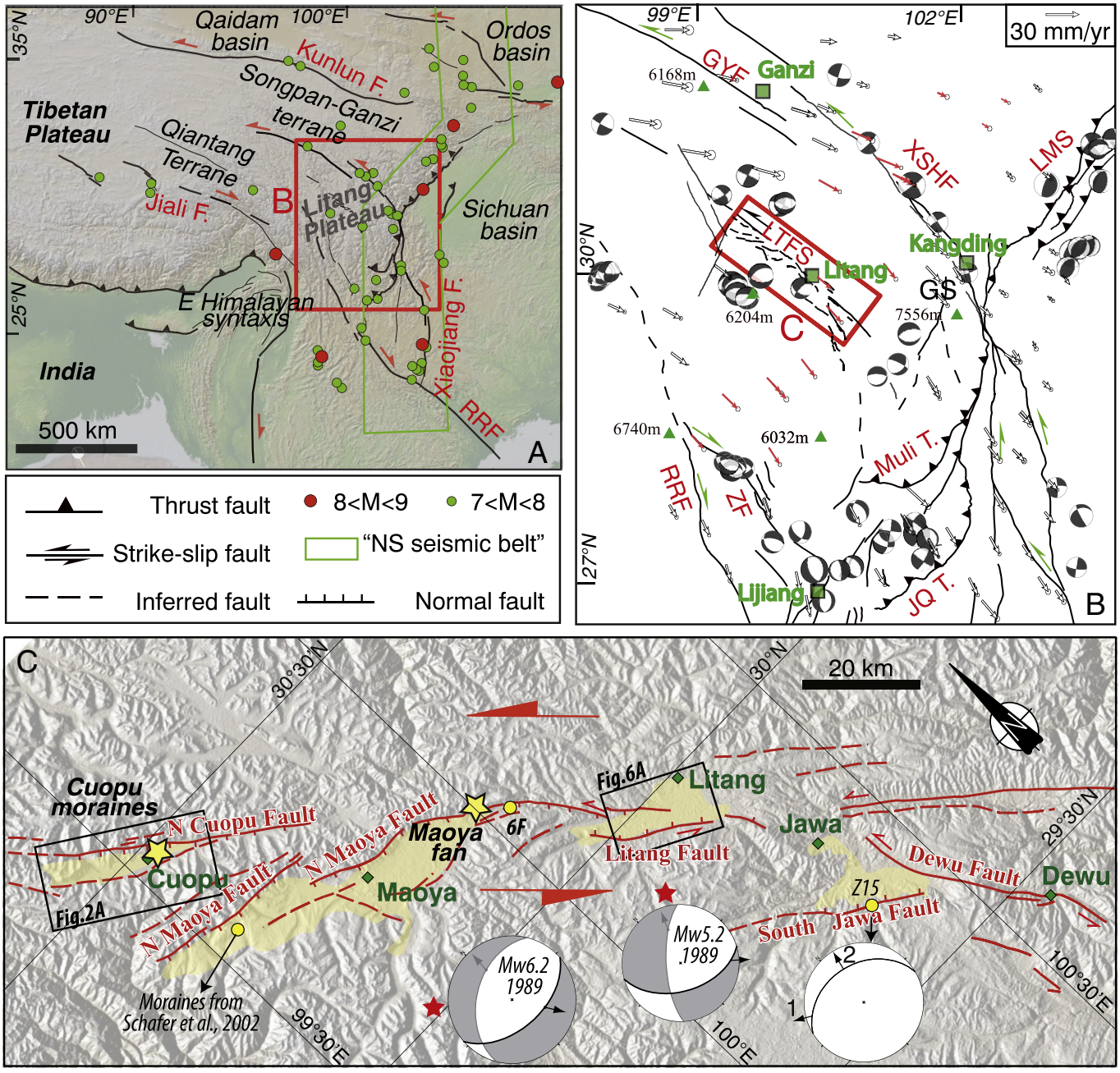

Fig. 1. The Litang fault system (LTFS) in the frame of the India–Asia collision zone. (A) Tectonic map of the eastern Himalayan syntaxis region with DEM in the background. Historical earthquakes of 9 > M > 7 are plotted and the "NS seismic belt" of Deng et al. (2003) highlighted by the green polygon. RRF = Red River fault. (B) SE Tibetan Plateau with horizontal GPS velocities (red arrows are used in the profile of Fig. S3) relative to stable Eurasia (Liang et al., 2013), focal mechanisms of instrumental earthquakes with Mw ≥ 5 (CMT catalogue 1976–2016), as well as main peaks, cities and faults. LTFS = Litang fault system, GYF = Ganzi–Yushu fault, XSHF = Xianshuihe fault, LMS = Longmen Shan, GS = Gongga Shan, ZF = Zhongdian fault, JQ T = Jinhe–Qinghe thrust. (C) DEM of the Litang fault system region with Quaternary basins (in yellow) and active faults (in red). Yellow stars show locations of the two study sites (Maoya fan and Cuopu moraines). Focal mechanisms of earthquakes (lower hemisphere projection) and corresponding slip directions (arrow pointing in the direction of motion of the upper block) are from global CMT catalogue, with the nodal plane assumed to be the fault in black. Brittle fault plane along the South Jawa fault with two generations of striations is plotted with the same convention: "1" = left-lateral striations, "2" = downslip striations (Z15 = Zhang et al., 2015).

to a major fault reorganization in SE Tibet, with the activation of the Lijiang pull-apart basin and Zhongdian fault, as well as the southeastward propagation of the Xianshuihe fault along the Xiaojiang fault system at that time (Fig. 1A,B). Zhang et al. (2015) further suggested that the Xianshuihe and Zhongdian faults allowed eastward sliding of the Litang Plateau during the Pliocene, with the LTFS accommodating differential motion within that block (Fig. 1B). During the Miocene, regional shortening was absorbed by the NNE–SSW-trending Jinhe–Qinghe and Muli thrust systems (Fig. 1B) (Yalong–Yulong thrust belt of Liu-Zeng et al., 2008). Such alternation between thickening and lateral motion along strike-slip faults is in agreement with the "hidden plate-tectonic" model (e.g., Tapponnier et al., 2001) which emphasizes the role of strike-slip faults. Alternatively, present-day normal faults could also be explained by a viscous lower crustal flow originating from the thick central Tibetan Plateau toward its thinner edges around the Sichuan rigid block (e.g., Clark and Royden, 2000; Schoenbohm et al., 2006). For this case, numerical simulations predict that the minimum horizontal stresses (direction of extension) would be parallel to the flow near the plateau margins and perpendicular to the flow out of the high plateau due to divergence of the flow where it spreads out

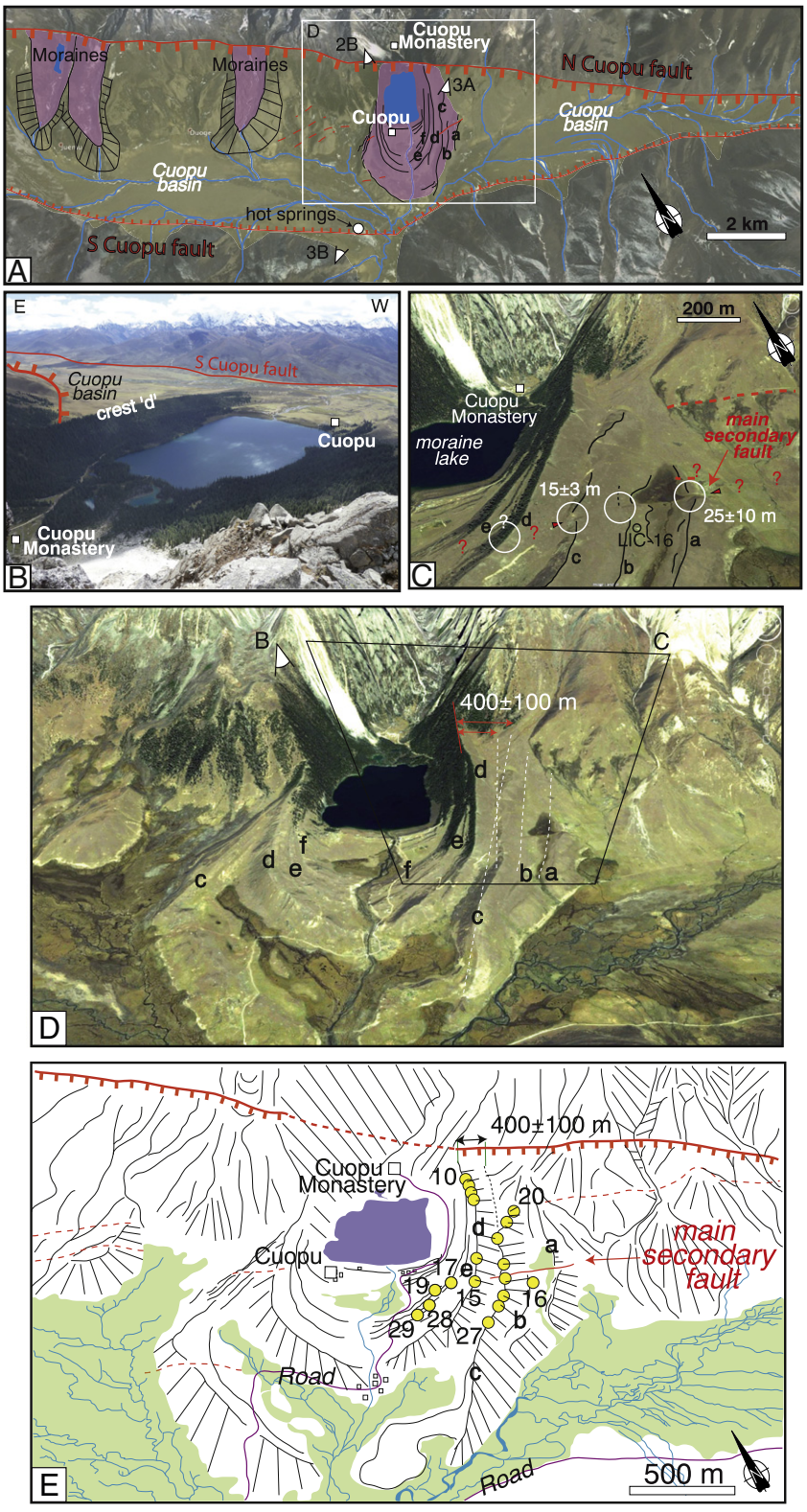

Fig. 2. The Cuopu basin. (A) Google Earth satellite image of the Cuopu basin with main geomorphic features. Moraines in pink (a-f correspond to the main moraines from older to younger), rivers in blue, active faults in red. (B) Aerial view of the moraine lake and ~4 km-long Cuopu moraine complex. (C) Close-up of eastern moraine crests (approximate box in D) offset by the main secondary fault (see field photos in Fig. 3). (D) Close-up of the Google Earth satellite image in 3D (approximate box in A) with offsets along the range-front fault (N Cuopu fault). (E) Interpreted map of (D). ^{10}Be cosmogenic samples and associated names (e.g., LIC-10) shown by yellow circles.

(Copley, 2008). While some regional focal mechanisms are compatible with such a model (Copley, 2008) (Fig. 1B), the strike and kinematics of the Litang and Xiaojiang fault systems, as well as that of the Lijiang pull-apart basin, seem to be less compatible with this lower crustal flow model. However, the Quaternary kinematics of these fault systems still need to be better characterized.

Despite its key location, few late Quaternary studies have been conducted in the Litang Plateau region. Our first observations imply that the

LTFS is a transtensive left-lateral fault system, with the ratio of normal and strike-slip components of motion varying with time and along the various fault segments (Zhang et al., 2015). However, many questions remain unanswered, in particular regarding the late Quaternary to present-day LTFS horizontal and vertical slip-rates. After describing the tectonics of the region and that of the LTFS in particular, we present two study sites along the LTFS: horizontally offset moraine crests from the Cuopu basin and a vertically offset alluvio-glacial fan from the eastern Maoya basin (stars in Fig. 1C). We use a combination of high-resolution satellite image observations and field surveys, as well as ^{10}Be cosmogenic surface-exposure dating of the offset geomorphic surfaces to constrain a late Quaternary slip-rate along the Cuopu and Maoya segments of the LTFS, and discuss our results in the frame of eastern Tibet's tectonics.

2. Geological setting

2.1. The Litang fault system (LTFS)

The NW-striking Litang fault system (LTFS) is located between two major fault systems in eastern Tibet, the left-lateral Xianshuihe fault system to the north, and the right-lateral Red River fault system to the south (XSHF and RRF in Fig. 1B). The LTFS lies within the high-elevation (4000–4500 m a.s.l.), low-relief Litang Plateau located in NW Sichuan province, and is ~190 km long, ~25 km wide, and discontinuous (Fig. 1C). It is mostly parallel to the highly active Xianshuihe fault, with both faults veering toward a southerly strike to the SE (Fig. 1B). The LTFS consists of four right-stepping en-echelon left-lateral/normal fault segments (each ~25–50 km long, striking ~N135°E) and four en-echelon rhomb-shaped basins filled with Quaternary sediments (yellow in Fig. 1C). From NW to SE, these are Cuopu, Maoya, Litang, and South Jawa-Dewu.

The LTFS is very active, with 3 historical earthquakes of $7.5 > M > 7$ since 1700. Xu et al. (2005) suggested, using tree rings counting on trees growing on the youngest scarps, that the last large earthquake along the Maoya segment occurred in 1886 (Ms7.1), despite the fact that no clear surface rupture has been found along that segment. In contrast, several well-preserved surface ruptures are present along the Litang and South Jawa-Dewu segments. While it had been suggested (e.g., Xu, 1979) that the 1948 earthquake (Ms7.3) had ruptured both the Litang and South Jawa-Dewu segments of the LTFS with ~70 km of surface ruptures, others suggested that this earthquake occurred only along the South Jawa-Dewu segment, with 41 km of surface ruptures (Xu et al., 2005; Zhou et al., 2015). This other interpretation is partly based on the presence of a 7–11 km gap between the two ruptures, and on the fact that the surface ruptures along the South Jawa-Dewu segment look much fresher than those along the Litang segment. Xu et al. (2005) suggested that the last large earthquake along the Litang segment occurred in 1890 (Ms7.1) with ~50 km of surface ruptures and Zhou et al. (2015) determined, using ^{14}C dating from a trench in the Litang basin, that a 25 km-long rupture was produced by an earlier event, the 1729 Mw6.7 Litang earthquake (or possibly by an older one, between 1420–1690). Along all segments of the LTFS, numerous evidence of tectonic activity are observed such as normal fault scarps, left-laterally offset geomorphic features, triangular facets, beheaded channels and shutter ridges, which all attest that the LTFS is a transtensive left-lateral fault system at present. We describe this evidence from NW to SE.

2.2. Cuopu basin

To the NW, the Cuopu basin (~25 × 4 km, trending ~N120°) is bounded by the N Cuopu and S Cuopu normal faults, the former being the master fault. Indeed, among this fault system, the Cuopu basin has the largest elevation difference (~1700 m) between its floor and the highest peak of the bounding mountain range to the north, attesting to the important normal component of motion of the N Cuopu fault. This present-day active fault is following the range-front, where steep fault planes with down-dip striations have been observed (Zhang et al., 2015). In contrast to the eastern half of the basin, very large and well-preserved moraines are present in the western half (pink in Fig. 2A). A large moraine lake is present in the center of the basin, surrounded by >5 frontal and lateral moraine crests ('a' to 'f' in Fig. 2). Hot springs are present in the center of the basin (Fig. 2A) and along the valley draining the basin toward the SW, most likely related to faulting activity along several ~EW-striking secondary faults located in the basin to the east and to the west of the moraine lake, as well as along the Cuopu normal faults bounding the basin. The main secondary fault cuts and left-laterally offsets the oldest moraine crests (i.e. farther away from the lake) (Figs. 2 and 3), and it also dams a small pond to the east (Figs. 2C and 3), due to its slight normal component of motion.

Regarding long-term rates, Zhang et al. (2015), using low-temperature thermochronology and 3D modeling (Pecube), determined that the vertical (exhumation) rate of the N Cuopu fault footwall increased from 0.005 to 0.99 ± 0.04 mm/yr at 5.3 ± 0.4 Ma, thus implying a vertical rate of ~1 mm/yr across the fault since the lower Pliocene. They also noted that the local geological map shows a possible maximum left-lateral offset of Triassic beds of ~11 km across the Cuopu segment (Bureau of Geology and Mineral Resources, 1991), and estimated a possible long-term left-lateral slip-rate of ~2 mm/yr.

2.3. Maoya basin

The Maoya basin is the largest basin along the LTFS (~50 × 10 km, trending ~N110°), located just SE of the Cuopu basin (Fig. 1C). It consists of two sub-basins, the eastern one being the larger and lower (Fig. 4A). The Maoya basin is asymmetrical, with a steep, high and sharp-crested range and few active streams along the northern side, while the southern side of the basin is gently sloping, with long rivers (~10 km from where they enter the basin) feeding the basin (Fig. 4A). The Maoya range bounding the northern edge of the eastern basin is sharp-crested with elevations up to ~5200 m in the NE, i.e. >1000 m higher than the basin's floor which lies at ~4100 m. U-shaped glacial valleys and moraines are particularly impressive on the northern flank of the western basin, where one present-day glacier remains, hanging from the highest peak. Numerous triangular facets attest to the normal component of the N Maoya fault, as well as vertical scarps cutting late Quaternary geomorphic features (Fig. 4A,B) that are visible along most of the northern edge of the basin, attesting to its recent normal faulting activity. In contrast, active faults are harder to follow along the southern edge of the basin, implying that the master fault is represented by the two N Maoya faults.

At the eastern end of the basin, well-developed alluvio-glacial fans cut by prominent fault scarps are ideal sites to study late Quaternary slip-rates as well as long-term exhumation rates. Xu et al. (2005) observed that one of these fans (Fig. 5) appears to be left-laterally and vertically offset by the N Maoya fault, and determined a Holocene left-lateral slip-rate of 4.1 ± 0.9 mm/yr and a reverse slip-rate of 1.8 ± 0.5 mm/yr using thermoluminescence dating. This sense of motion is however not in agreement with the basin morphology, attesting to normal motion (Zhang et al., 2015). Using low-temperature thermochronology (apatite and zircon fission track as well as apatite (U–Th)/He dating), Zhang et al. (2015) determined an increase in vertical (exhumation) rate up to 0.59 ± 0.03 mm/yr (normal, not reverse) at 6.6 ± 0.5 Ma. They interpreted this age to correspond to the initiation age of the N Maoya fault. Regarding long-term offsets, Zhang et al. (2015) noted that the Upper Triassic Ganzi–Daocheng pluton is left-laterally offset by ~6 km across the Maoya segment and estimated a possible long-term left-lateral slip-rate of ~0.9 mm/yr.

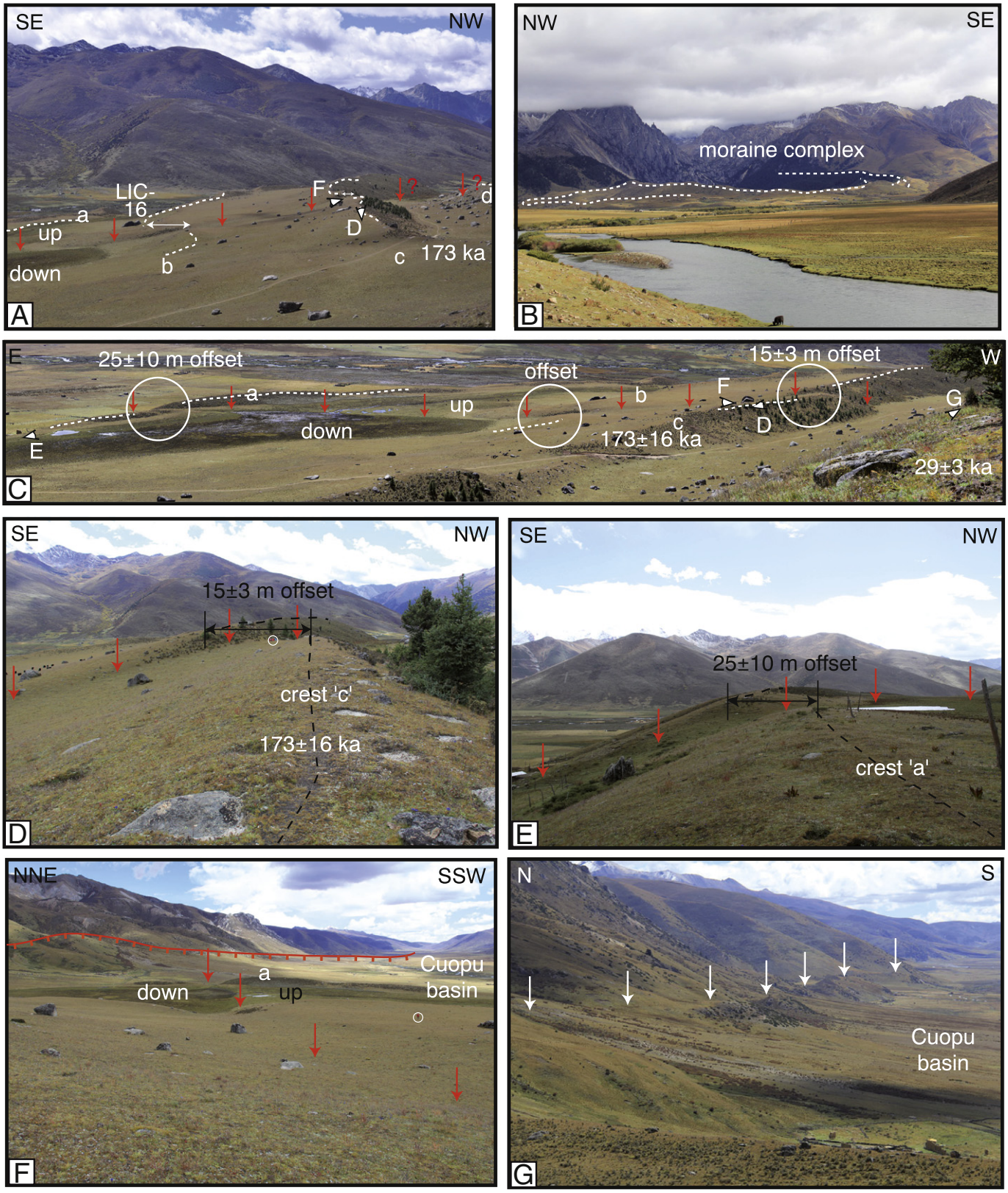

Fig. 3. Field photos of the Cuopu basin. (A) View looking at the three moraine crests (a, b, c) offset by the main secondary fault (red arrows). Sample LIC-16 (big boulder) is visible near 'b'. (B) Photo of the entire Cuopu moraine complex. (C) Panoramic photo showing the main secondary fault offsetting the 3 oldest moraine crests by 25 ± 10 m (crest 'a') and 15 ± 3 m (crest 'c'). Crest 'b' is harder to realign across the fault because it is highly degraded. Sag ponds are present between 'a' and 'b' due to the minor normal component of the fault. (D,E) Close-up of the offset moraine crests. Locations shown in (C). (F) View of the main secondary fault toward the range-front fault, highlighting its slight normal component. (G) Secondary fault near the N Cuopu normal fault (range-front fault) shown by white arrows (see Fig. 2E). Person circled for scale in (D) and (F).

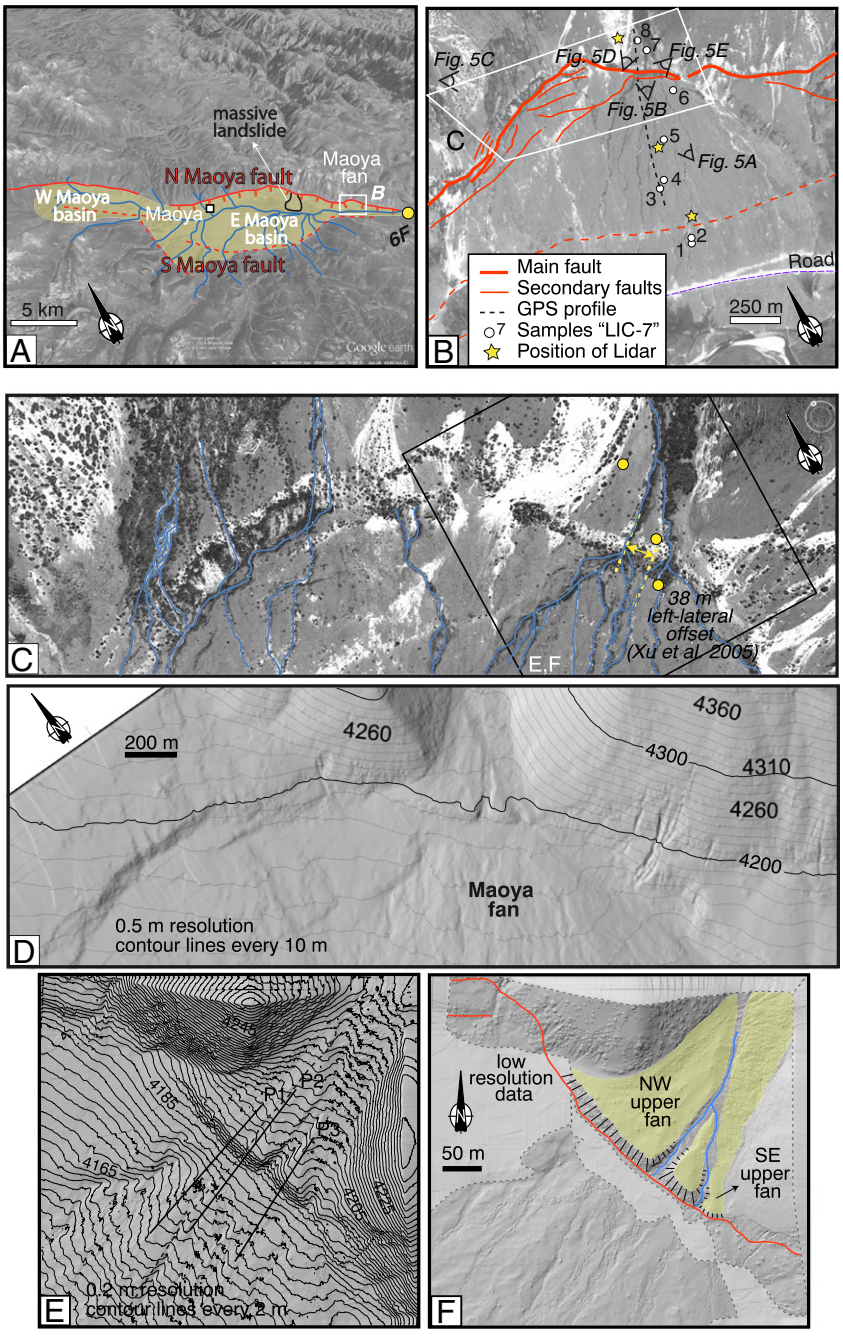

Fig. 4. The Maoya basin. (A) 3D Google Earth satellite image (3× vertical exaggeration) of the Maoya basin (B). Maoya fan site with active faults, kinematic GPS profile (Fig. 8A), position of LiDAR bases, collected samples (LIC-), and locations of photos from Fig. 5 are shown. (C) Close-up of the main fault scarp (approximate box in B), with active streams/gullies network highlighted in blue, attesting that no clear left-lateral offset is visible, despite the 38 ± 7 m offset suggested by Xu et al. (2005) (yellow dashed lines). Yellow circles show location of Xu et al. (2005) thermoluminescence samples. (D) 0.5 m resolution LiDAR data of the fault scarp. (E,F) 0.2 m resolution LiDAR data (box in C) with location of LiDAR profiles in Fig. 8B, and that of kinematic GPS profile in Fig. 8A (dashed line).

2.4. Litang basin

In the NW Litang basin (20 × 10 km, ~N135°), linear surface ruptures are still visible and well-preserved (Xu et al., 2005; Zhou et al., 2015; Zhang et al., 2015; Fig. 6B,C), due to the last large earthquake that occurred along the Litang segment in 1890 (Ms7.1, 50 km of ruptures, Xu et al., 2005) or in 1729 (Mw6.7, 25 km of ruptures, Zhou et al., 2015). The rupture still displays left-laterally offset gullies of up to ~1.8 m with a cumulative vertical offset of ~3 m, attesting to the currently transtensive kinematics of the LTFS (Zhang et al., 2015). The southern side of the basin has a steeper topography (with elevation difference between the peaks and the basin floor of >1000 m), several U-shaped valleys, moraines and shutter ridges and fault scarps attesting to its normal component of motion (Fig. 6). Regarding long-term offsets, Zhang et al. (2015) noted that Paleozoic rocks overlain by Eocene basins show a 14 km left-lateral offset across the Litang segment. Assuming that the Litang fault initiated at the same time as the nearby N Maoya fault (6.6 ± 0.5 Ma) would lead to a left-lateral slip-rate of 2.1 ± 0.2 mm/yr.

2.5. Jawa basin

Towards the SE end of the LTFS, the Jawa basin (20 × 15 km, ~N130°) is bounded by the linear Dewu fault to the east and by the South Jawa fault to the SW (Fig. 1C). The 1948 earthquake occurred along the former (with still visible surface ruptures) and a left-lateral late Quaternary slip-rate of ~4 mm/yr was suggested by Xu et al. (2005), using thermoluminescence dating of an offset alluvial fan. Along the South Jawa fault, fault plane striations suggest that normal faulting kinematics could dominate the LTFS at present, following a previously dominant left-lateral kinematics in the past (Zhang et al., 2015). Southeast of the Jawa basin, the LTFS changes direction to become more NS-striking and its trace becomes difficult to follow on the satellite images as well as in the field.

3. Methodology

We used field observations, Google Earth satellite images, high-resolution topographic data from a Riegl VZ1000 terrestrial LiDAR (Light Detection and Ranging) scanner (Fig. 4D–F) (angular resolution of 0.02° for raw data, set to <0.5 m between two data points after process), as well as from a kinematic GPS (Trimble R8) at the Maoya fan site, in order to map active fault strands and geomorphic surfaces, and to precisely measure offsets. We used ^{10}Be cosmogenic dating to determine the surface-exposure age of 19 granite samples collected using chisel and hammer to chop off the top few centimeters of large boulders present on the Cuopu moraine crests (Fig. S1), and 8 large granite boulders from the Maoya alluvio-glacial fan surface (Fig. S2) in order to determine the surface emplacement ages (Fig. 7 and Table 1). Matching the age of the surfaces with their offset yields average slip-rates (calculated using Zechar and Frankel, 2009) at the late Quaternary timescale, to be compared with rates at shorter and longer timescales.

4. Site description and results

4.1. Cuopu moraines

The particularly impressive Cuopu moraines are located in the center of the Cuopu basin (Fig. 2A) at 30.485°N–99.54°E, at an elevation of ~4150 m. The youngest crests are observed close to the lake and are mostly continuous except where they have been breached by the stream originating from the lake. The oldest moraines ('a' and 'b') are found farther from the lake and only on the east side. The N Cuopu master fault runs along the range-front (Fig. 2A) and does not vertically offset the moraines as they are only present south of the fault in the basin (in the master fault's hanging wall), thus no estimate of the vertical offset of the moraines on that fault can be determined. The fact that the oldest moraines do not, at present, stand in the prolongation of the valley from where the glacier originated, but in front of triangular facets, suggests a left-lateral motion on the master fault (Fig. 2D,E). An ~EW-striking secondary fault cuts and horizontally offsets the three oldest moraine crests. The offset is 15 ± 3 m for crest 'c' (measured by handheld GPS, plotted and measured on Google Earth) and 25 ± 10 m (measured on Google Earth) for crest 'a' which is not as sharp (Figs. 2C and 3). The offset of crest 'b' is harder to measure due to its highly degraded crest along which no boulder remains (except LIC-16). Minor vertical displacement created sag ponds between moraines 'a' and 'b' (Fig. 3). Overall, the three crest offsets appear to be compatible, with crest 'a' offset by a larger amount, in agreement with moraines' relative chronology, where crest 'a' is older than crest 'c'. Note that while this requires further field investigation (hard to constrain on the satellite images alone), crest 'd' could be slightly affected by the main secondary fault (Fig. 2C). The younger moraines close to the lake however do not appear offset, suggesting fault activity only prior to the emplacement of moraine 'd' (or 'e'). East of the oldest preserved moraine, a recent, undisturbed alluvial fan has most likely destroyed other possible evidence of fault traces and offsets (Fig. 2C). While west of the lake, the youngest moraines show no offsets, the oldest ones appear disturbed by the fault, even though no clear offset could be mapped (Fig. 2A,E).

We collected 19 samples from crests 'b–f' (Figs. 2E, 7A and Table 1), but only one sample has been dated on crests 'b' and 'f'. Ages from crest 'c' range from 48 to 173 ka (number of samples = 8), from 15 to 29 ka on crest 'd' (n = 6) and are ~16 ka on crest 'e' (n = 3) (Fig. 7A). We choose the oldest age on each surface to represent the moraine emplacement age to account for the numerous processes that can lead to apparent young ages: erosion, weathering, spallation, snow cover and rolling (e.g., Putkonen and Swanson, 2003; Applegate et al., 2010; Chevalier et al., 2011; Heyman et al., 2011). While inheritance (or prior exposure), which yields apparent old ages, may also have affected the samples we collected, it has been shown that the percentage of boulders that were exposed prior to glacial erosion (as well as transport and deposition) is quite small (<3%) (Putkonen and Swanson, 2003; Heyman et al., 2011), and that those outliers have ages that are much older than the rest of the samples. Therefore, our choice of taking the oldest age is validated since no anomalously old sample is present here, except maybe on crest 'd' (sample at 29 ka while the rest are ~17 ka, see discussion below). In addition, a moraine surface may be unstable after its emplacement, with large boulders being exhumed to the surface as erosion transports the finer material away (e.g. Hallet and Putkonen, 1994; Putkonen and Swanson, 2003; Briner et al., 2005; Applegate et al., 2010; Heyman et al., 2011). These gradually exhumed boulders therefore represent different stages of exhumation as the surface lowers. Crest 'c' being quite smooth and irregular compared to crests 'd–f', it is likely to have been affected by such processes. Assuming negligible prior exposure as explained above, the oldest age of the surface therefore better represents the emplacement age of the moraine (e.g. Hallet and Putkonen, 1994; Putkonen and Swanson, 2003; Briner et al., 2005; Applegate et al., 2010; Chevalier et al., 2011; Heyman et al., 2011). One could instead imagine that the majority of boulders on crest 'c' is made of outliers that were picked up, transported and deposited by the glacier to the crest. However, prior exposure is often limited because glacial boulders have most likely been pulled off from the glacial valley, crushed, and eroded.

Moraine emplacement ages are therefore 69 ± 6 ka on crest 'b', 173 ± 16 ka on crest 'c', 29 ± 3 ka on crest 'd', 16 ± 1 ka on crest 'e' and 15 ± 1 ka on crest 'f'. Crest 'b' is located the farthest away from the moraine lake and should therefore be the oldest, which is not the case. There, only one sample (LIC-16) was collected (not statistically sound) from the broad crest due to the lack of other suitable boulders (Fig. 3A). We believe it has most likely been affected by erosion (surface lowering due to matrix erosion or boulder toppling, yielding lower ^{10}Be concentration) and may be discarded (outlier in white in Fig. 7A) (e.g., Benedetti and Van der Woerd, 2014). However, even though only one sample has also been collected on the youngest (sharpest) sampled crest 'f' (therefore also not statistically sound), its age is in agreement with moraines' relative chronology, where younger moraine crests (especially 'e', 'f' and other younger crests closer to the lake) are harder to differentiate from one another, due to their close proximity.

The Cuopu moraines are located in the monsoon-influenced part of the Tibetan Plateau, as defined by Owen et al. (2008). Moraine crest 'c' at 173 ± 16 ka would correspond to Marine Isotope Stage MIS-6. This is similar to the oldest moraine age determined so far in SE Tibet: 184 ± 17 ka at Nata site located 42 km due north of Cuopu (Fu et al., 2013). Moraine crests 'e–f' at ~16–15 ka were emplaced during the Heinrich 1 event by glacier retreat following the Last Glacial Maximum (LGM, MIS-2, ~20 ka) (Fig. 7A). These ages are consistent with nearby studies (Schafer et al., 2002; Xu and Zhou, 2009 and Fu et al., 2013) who dated moraine crests at ~16 ka in the west Maoya basin (location in Fig. 1C) and in the nearby Shaluli Mountains, respectively. Lastly, crest 'd' appears to belong to MIS-3/2, even though one may consider

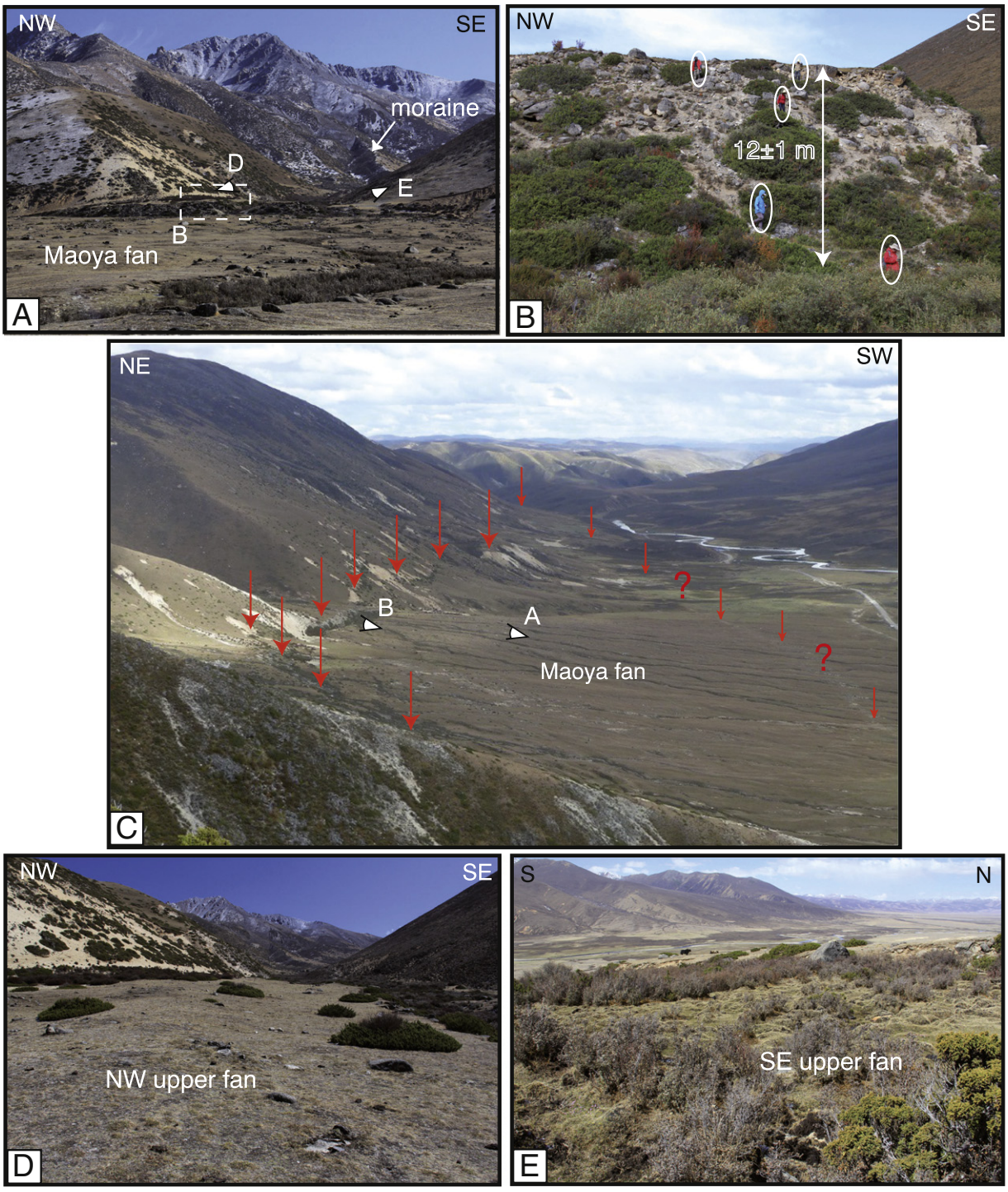

Fig. 5. Field photos of the Maoya fan site. (A) View of the steep scarp on the Maoya fan with upstream moraine in the background. (B) Close-up of the fault scarp (12 ± 1 m) with people circled for scale. (C) Aerial view looking east, of the Maoya fan and eastern Maoya basin. The N Maoya fault and a possible secondary fault are marked by red arrows. (D) View of the NW upper fan surface (where sample LIC-8 is located, Fig. 4B). Note how flat and bare it is compared to the SE upper fan surface, which has marshes and much denser vegetation (E).

LIC-10 (29 ka) to be an outlier (because much older than the next oldest age, i.e. possibly affected by inheritance, Putkonen and Swanson, 2003), yielding the oldest age on 'd' to become 17 ± 2 ka (MIS-2), slightly older than moraine crests 'e' at 16 ± 1 ka and 'f' at 15 ± 1 ka, and still in agreement with moraines' relative chronology. Matching the 15 ± 3 m horizontal offset with the 173 ± 16 ka age of the offset moraine crest 'c' yields a poorly constrained, very small left-lateral slip-rate of 0.09 ± 0.02 mm/yr along the main secondary fault at Cuopu. One could also view the oldest sample on crest 'c' (LIC-25 at 173 ± 16 ka) as an outlier so that the next oldest age (LIC-20 at 145 ± 13 ka) better represents the moraine's age, yielding a slightly higher left-lateral slip-rate of 0.1 ± 0.03 mm/yr.

4.2. Maoya fan

The Maoya fan site is located along the Maoya segment of the LTFS (Fig. 1C), at 30.176°N-100°E, at an elevation of ~4230 m. It lies at the eastern end of the eastern basin, where the basin becomes narrower (~1 km as opposed to a maximum of 10 km farther west). The <3 km-long valley from where the Maoya fan originates cuts

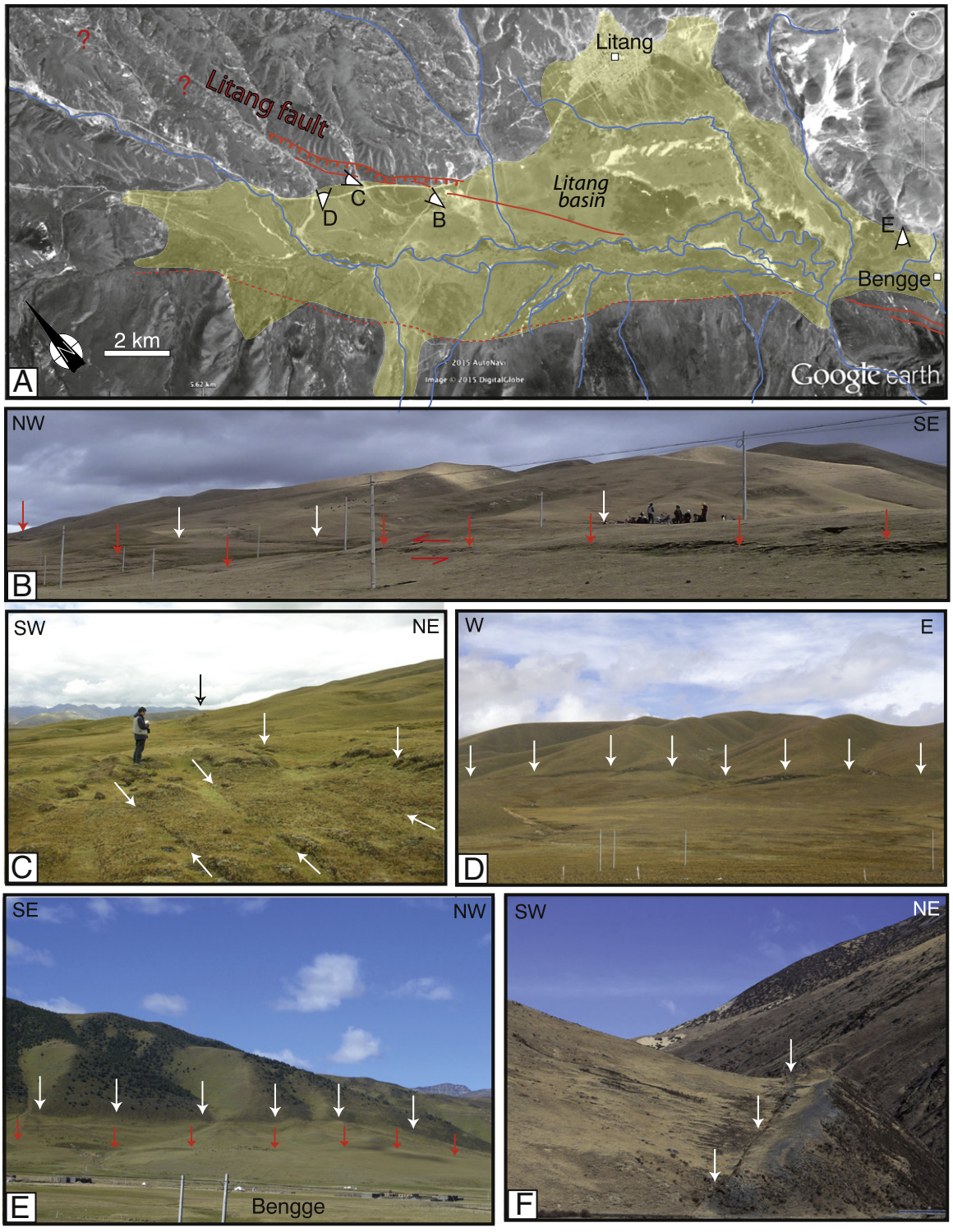

Fig. 6. The Litang basin. (A) Google Earth satellite image of the Litang basin. (B–D) Photos of the most recent surface rupture (1890 Ms7.1, Xu et al., 2005 or 1729 Mw6.7, Zhou et al., 2015) located in the NE part of the basin. (E) Litang fault at the southern end of the Litang basin (Bengge). (F) Litang fault just east of the Maoya basin. Photo location shown in Fig. 1C. White arrows highlight fault with main normal component while red arrows highlight fault with main left-lateral component.

through the northern Maoya range. The stream flowing through the valley most likely originates from springs located ~300 m higher than the fault, as well as from precipitation and seasonal snowmelt. In addition, two former glacial valleys (with no present-day glacier) are perched ~500 m higher than the valley upstream from the Maoya fan. In particular, moraines from the eastern one reach the valley floor just ~700 m upstream from the Maoya fan (Fig. 5A) and may attest to the largest glacial extent. Therefore, we believe that the Maoya fan is an alluvio-glacial fan surface, which most likely emplaced almost instantaneously, following the frontal moraine's collapse and depositing exceptionally large boulders on the fan downstream.

The Maoya alluvio-glacial fan surface (~8° slope to the SW) is entrenched by several gullies (Fig. 4C), mostly seasonally active, that reach the Litang River crossing the basin in an ~EW direction (Fig. 4A).

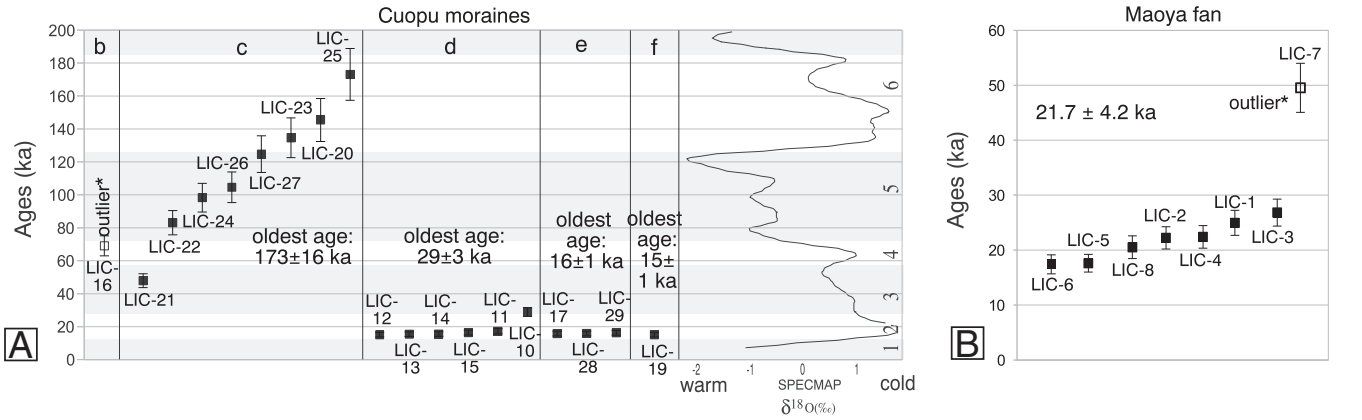

Fig. 7. Ages of Cuopu moraines and Maoya fan. ^{10}Be cosmogenic surface-exposure ages (using the Lal (1991)/Stone (2000) time-dependent model, bold in Table 1, "LS dep" column) with 1-sigma (s) uncertainty for (A) the Cuopu moraines and (B) Maoya fan sites. Note the outliers in white (see text for details). The average age of each surface is calculated at the 1-sigma (s) level using Zechar and Frankel (2009). Specmap climatic proxy curve to the right in (A), with gray-shaded sectors showing the Marine Isotope Stages (MIS) of Imbrie et al. (1984).

The Maoya fan surface is covered by short grass (Fig. 5), but small bushes abound where water is present (Figs. 4C and 5A), especially in the SE upper fan surface (Fig. 5E). Indeed, the upper fan surface is deeply entrenched by two active streams that separate it into three different surfaces. The western and central upper surfaces are flat and almost devoid of vegetation (Fig. 5D) while the SE upper surface is highly vegetated with marshes (Fig. 5E). The upstream part of the Maoya fan is small and narrow (~100–200 m wide and ~200 m long) compared to the downstream part (~1 km wide and ~1.2 km long) (Fig. 4).

The N Maoya fault cuts and vertically offsets numerous alluvial fans near their apex, including the Maoya fan and a similar fan just to the west (Fig. 4). Another trace, possibly a secondary fault, cuts the Maoya fan farther downstream (Figs. 4B and 5C). The main fault scarp has a slope of ~35° and is partly covered by bushes (Fig. 5B). We leveled a kinematic GPS profile perpendicular to the scarp (Fig. 4B,E), which allowed us to precisely measure the vertical offset of the Maoya fan of 12 ± 1 m (Fig. 8A), value confirmed by our terrestrial LiDAR survey (Figs. 4D–F and 8B). We collected eight samples from large boulders rapidly emplaced following the upstream moraine's breach, two upstream (LIC-7, 8) and six downstream (LIC-1-6) from the fault (Figs. 4B and S2), with ages ranging from 18 to 50 ka (Fig. 7B and Table 1). Sample LIC-7 (50 ± 4 ka) is twice as old as the rest of the samples and may have been affected by inheritance (or prior exposure) (Fig. 7B). Indeed, while for large catchments it has been suggested that inheritance is evenly distributed in all the samples (Hetzel et al., 2002), in smaller catchments however, inheritance can usually be assessed by the occurrence of outliers (with an age much older than the rest of the population) that can thus be discarded (e.g. Van der Woerd et al., 1998) (white in Fig. 7B). Whether the other samples may have been affected by inheritance as well is hard to assess without sampling the active river or by doing a depth profile. The remaining seven samples yield an average age of 21.7 ± 4.2 ka, which, when matched with the 12 ± 1 m vertical offset yields a vertical rate of 0.6 ± 0.1 mm/yr for the Maoya segment of the LTFS.

The fact that the age of the Maoya fan corresponds to the Last Glacial Maximum (LGM, ~20 ka) is in agreement with our inference that the Maoya fan is an alluvio-glacial fan which emplaced rapidly, possibly due to a glacial lake outburst flood that breached the frontal moraine located upstream from the fan (due to water pressure, earthquake, erosion, rock or snow avalanches etc). This also reinforces our preference for the Maoya fan to be 22 ka rather than ~10 ka, as suggested by Xu et al. (2005).

5. Discussion

5.1. Horizontal rate along the Cuopu segment

The Cuopu moraines are only found on one side of the main range-front fault (N Cuopu fault), which prevents us to determine a vertical rate along this main fault segment. However, a left-lateral rate along the main secondary fault affecting the moraines can be calculated. Matching the 173 ± 16 ka old moraine crest ('c') with its 15 ± 3 m left-lateral offset by the main secondary fault within the basin yields a horizontal slip-rate of 0.09 ± 0.02 mm/yr (or 0.1 ± 0.03 mm/yr taking the next oldest age, 145 ± 13 ka, as discussed above). This rate is >20 times smaller than the ~2 mm/yr Pliocene rate obtained by matching the ~11 km long-term offset with the 5.3 ± 0.4 Ma fault initiation age (Zhang et al., 2015) (Fig. 9). However, this long-term offset has most likely been accumulated along the range-front fault, which appears as purely normal at present. Indeed, the oldest moraine crests 'a,b,c' east of the lake are now facing triangular facets, most likely due to left-lateral displacement of moraines previously located in front of the glacial valley. Furthermore, no corresponding crests for 'a' and 'b' are present west of the lake due to left-lateral motion along the range-front (younger moraines have easily destroyed older ones that were facing the valley, e.g., Chevalier et al., 2005, 2015). It is hard however to calculate a precise horizontal slip-rate for the N Cuopu fault due to the lack of piercing point for moraines 'a,b,c' due to erosion by fans located upstream (Fig. 2C). Nevertheless, an attempt to project the crests toward the range-front (Fig. 2D), or taking the distance between crests 'd' and 'c' yields a first order slip-rate estimate of 2.3 ± 0.6 mm/yr (400 ± 100 m in 173 ka), similar to the Pliocene rate. If one assumes that LIC-25 (173 ± 16 ka) is an outlier and that LIC-20 (145 ± 13 ka) better represents the moraine's age, the rate becomes 2.8 ± 0.9 mm/yr.

In addition, the presence of horizontal offsets on the oldest moraine crests only, and not on the youngest ones nor on the alluvial fan to the east, suggests that the main secondary fault was only active in the past and stopped before the younger moraines (and fan) emplaced (sometimes between ~173 and ~29 ka, or 17 ka). If our hypothesis of a cessation of left-lateral active faulting along both the N Cuopu and secondary fault is correct, it could be compared to what happens along the South Jawa fault, where the fault plane shows older left-lateral striations crosscut by younger, normal ones (Zhang et al., 2015), attesting that strike-slip motion preceded normal motion. At present, only the N Cuopu fault remains active, with a pure normal sense of motion.

Table 1
Analytical results of ^{10}Be geochronology and surface exposure ages at Maoya fan and Cuopu moraines.

	Sample name	Lat (N)	Long (E)	Elev (m)	Quartz (g)	Be carrier (mg)	^{10}Be/^{9}Be (10^{-15})	^{10}Be (10^{6} atom/g)	Desilets ages (yrs)[a]	Dunai ages (yrs)[a]	Lifton ages (yrs)[a]	LS indep ages (yrs)[a]	**LS dep ages (yrs)[a]**
Cuopu moraines													
b	LIC-16	30.481064	99.555136	4176	19.66575	0.29445	4129 ± 68	4.13 ± 0.068	63931 ± 7777	62694 ± 7590	60160 ± 6135	80543 ± 7317	**69047 ± 6069**
c	LIC-21	30.48852	99.55858	4243	20.53443	0.30149	3089 ± 55	3.03 ± 0.053	44078 ± 5333	43282 ± 5213	41829 ± 4248	56932 ± 5143	**47938 ± 4195**
	LIC-22	30.48642	99.55575	4222	20.11649	0.29881	5044 ± 92	5.006 ± 0.091	76097 ± 9314	74253 ± 9043	71302 ± 7320	96832 ± 8878	**83079 ± 7366**
	LIC-24	30.48206	99.55309	4193	20.80545	0.29816	6163 ± 93	5.901 ± 0.089	91089 ± 11165	88848 ± 10833	85317 ± 8754	115722 ± 10607	**98276 ± 8697**
	LIC-26	30.47865	99.54978	4190	19.33687	0.29754	6127 ± 94	6.299 ± 0.097	97211 ± 11944	94990 ± 11611	91769 ± 9442	124578 ± 11461	**104612 ± 9284**
	LIC-27	30.47812	99.54898	4181	20.61034	0.29695	7898 ± 117	7.603 ± 0.112	114782 ± 14177	111525 ± 13699	108273 ± 11191	151953 ± 14092	**124729 ± 11130**
	LIC-23	30.48384	99.55453	4199	20.2695	0.29839	8379 ± 122	8.242 ± 0.12	122759 ± 15201	118939 ± 14643	115614 ± 11977	164382 ± 15304	**134627 ± 12050**
	LIC-20	30.48948	99.55989	4246	19.63962	0.29368	9070 ± 126	9.062 ± 0.125	131061 ± 16262	126317 ± 15578	122620 ± 12718	176840 ± 16511	**145435 ± 13046**
	LIC-25	30.48031	99.55197	4186	21.04332	0.29784	10874 ± 150	10.284 ± 0.141	156483 ± 19583	150572 ± 18722	145146 ± 15169	208624 ± 19688	**173075 ± 15669**
d	LIC-12	30.49258	99.55746	4289	16.9111	0.2993	720 ± 21	0.851 ± 0.024	14589 ± 1779	15136 ± 1838	14078 ± 1452	15494 ± 1425	**15144 ± 1355**
	LIC-13	30.49138	99.55695	4279	18.3889	0.29779	800 ± 23	0.865 ± 0.024	14899 ± 1817	15430 ± 1874	14369 ± 1482	15848 ± 1458	**15460 ± 1384**
	LIC-14	30.48356	99.55147	4206	15.09584	0.29646	648 ± 19	0.85 ± 0.024	15016 ± 1831	15542 ± 1888	14483 ± 1494	15944 ± 1466	**15544 ± 1391**
	LIC-15	30.48244	99.55099	4198	19.95144	0.2954	905 ± 24	0.895 ± 0.024	15837 ± 1926	16339 ± 1979	15269 ± 1569	16923 ± 1548	**16412 ± 1461**
	LIC-11	30.49407	99.55808	4292	17.01552	0.29842	835 ± 29	0.978 ± 0.033	16506 ± 2038	16991 ± 2089	15895 ± 1667	17820 ± 1673	**17205 ± 1574**
	LIC-10	30.49535	99.55858	4296	16.1193	0.36928	1125 ± 36	1.721 ± 0.055	27311 ± 3370	27405 ± 3367	26083 ± 2729	31599 ± 2960	**28885 ± 2633**
e	LIC-17	30.48278	99.54843	4173	19.1385	0.29493	817 ± 24	0.84 ± 0.024	15284 ± 1865	15803 ± 1920	14747 ± 1522	16216 ± 1492	**15786 ± 1414**
	LIC-28	30.48145	99.54565	4156	19.82563	0.29672	833 ± 23	0.832 ± 0.023	15383 ± 1873	15899 ± 1928	14845 ± 1527	16307 ± 1495	**15866 ± 1415**
	LIC-29	30.48107	99.54456	4152	20.23429	0.29753	873 ± 27	0.857 ± 0.026	15774 ± 1932	16278 ± 1986	15216 ± 1579	16779 ± 1555	**16284 ± 1469**
f	LIC-19	30.48293	99.5475	4164	18.58772	0.29504	750 ± 21	0.795 ± 0.022	14690 ± 1789	15230 ± 1847	14184 ± 1460	15493 ± 1421	**15141 ± 1351**
Maoya fan													
Down	LIC-1	30.16814	99.99681	4119	17.2226	0.374297	912 ± 29	1.325 ± 0.042	24037 ± 2962	24296 ± 2982	23022 ± 2406	27020 ± 2526	**25092 ± 2283**
	LIC-2	30.16876	99.99728	4126	16.0895	0.370415	760 ± 24	1.169 ± 0.037	21500 ± 2647	21865 ± 2681	20599 ± 2151	23741 ± 2217	**22352 ± 2032**
	LIC-3	30.17122	99.9978	4150	16.7291	0.370549	984 ± 31	1.456 ± 0.046	25739 ± 3174	25940 ± 3185	24582 ± 2570	29258 ± 2738	**26964 ± 2455**
	LIC-4	30.17142	99.99828	4155	17.5306	0.367419	855 ± 28	1.197 ± 0.04	21635 ± 2673	21997 ± 2706	20726 ± 2174	23953 ± 2250	**22530 ± 2061**
	LIC-5	30.17257	99.99949	4177	18.1695	0.374478	677 ± 22	0.933 ± 0.03	17100 ± 2105	17578 ± 2155	16461 ± 1719	18431 ± 1722	**17715 ± 1612**
	LIC-6	30.17402	100.0018	4210	17.9985	0.366027	689 ± 35	0.937 ± 0.047	16889 ± 2182	17372 ± 2237	16260 ± 1815	18208 ± 1846	**17519 ± 1736**
Up	LIC-7	30.17643	100.00217	4252	18.8779	0.372542	2324 ± 64	3.065 ± 0.085	45533 ± 5600	44627 ± 5464	43060 ± 4473	59096 ± 5497	**49728 ± 4487**
	LIC-8	30.17686	100.00211	4261	19.8518	0.371066	918 ± 48	1.146 ± 0.06	19733 ± 2568	20158 ± 2614	18911 ± 2130	21739 ± 2229	**20639 ± 2069**

Note: Samples were processed at Stanford University's cosmogenic facility and the ^{10}Be/^{9}Be ratios were measured at ASTER (CEREGE).
Ages calculated with the CRONUS 2.2 (with constants 2.2.1) calculator. LS dep (indep) = Lal (1991) / Stone (2000) time-dependent (independent) production rate model.
Dunai (2000, 2001); Desilets and Zreda (2003); Desilets et al. (2006); Lifton et al. (2005).
Shielding factor is 0.98; sample density is 2.7 g/cm3. Thickness is ~5 cm. No erosion rate was applied.
Standard used at ASTER is NIST SRM4325 (=NIST_27900) with ^{10}Be isotope ratios = 2.79×10^{-11}, equivalent to 07 KNSTD.
[a] External uncertainties (analytical and production rate, Balco et al., 2008) are reported at the 1 σ confidence level.

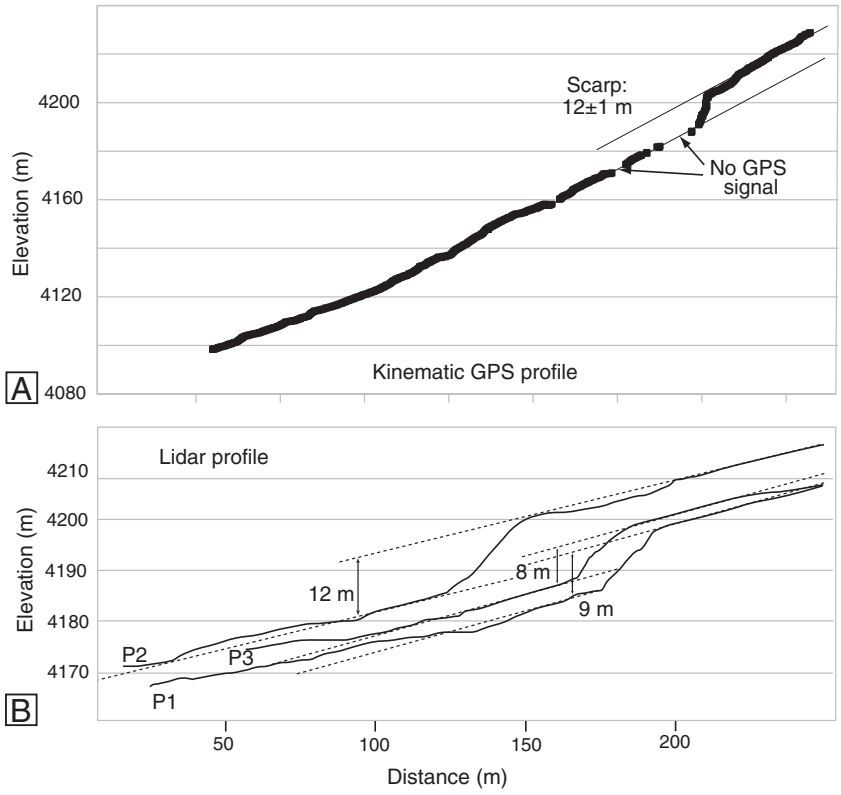

Fig. 8. Profile across the Maoya fan scarp. Profiles obtained by kinematic GPS (A) and LiDAR scanner (B) perpendicular to the Maoya fan (positions in Fig. 4B,E) showing the 12 ± 1 m vertical offset of the Maoya fan.

5.2. Vertical rate along the Maoya segment

Matching the 12 ± 1 m vertical offset of the Maoya fan (using kinematic GPS and LiDAR data) with its 21.7 ± 4.2 ka surface age, we determined a vertical rate of 0.6 ± 0.1 mm/yr (Fig. 9). At the same site, Xu et al. (2005) measured a 17 ± 3 m vertical (reverse) offset of the Maoya fan (using total station) and determined a 9.4 ± 0.42 ka surface age from three samples using thermoluminescence dating on sands collected beneath the modern soil. They therefore obtained a vertical (reverse) rate of 1.8 ± 0.6 mm/yr. Recalculating Xu et al. (2005)'s average age and slip-rate using Zechar and Frankel (2009) yielded 8.8(+2.8/−0.9) ka and 1.8(+0.5/−0.4) mm/yr, respectively. Their rate is three times as high as what we determined at the same timescale with a different technique. This difference in surface ages may simply reflect technique shortcomings, such as the fact that Xu et al. (2005) collected only three samples which location may not be ideal because they may have been reset by riser erosion or gully entrenchment, or small rockslides (yellow in Fig. 4C). In addition to our inference that the Maoya fan emplaced following the upstream moraine's breach (as explained above), we believe that the seven similar sample ages we obtained on the Maoya fan using ^{10}Be dating are more representative of its true age and therefore we favor a 21.7 ± 4.2 ka emplacement age and a lower rate, 0.6 ± 0.1 mm/yr. Furthermore, the sense of motion (reverse) suggested by Xu et al. (2005) is incompatible with our observations of the basin morphology, which attests of normal motion (Zhang et al., 2015), as explained above.

Xu et al. (2005) also argued that a now beheaded gully downstream from the fault has accumulated a left-lateral offset of 38 ± 7 m compared to the active stream, upstream from the fault (Fig. 4C), yielding a horizontal slip-rate of 4.1 ± 0.9 mm/yr, or 4.1(+2.2/−1.8) mm/yr using Zechar and Frankel (2009). Our detailed streams/gullies mapping and field survey however casts doubts on this left-lateral offset. Indeed, while the gullies network appears to be disturbed by the scarp, our observations show no tectonic lateral offset (Fig. 4C). Past the scarp, the streams fan out on the lower fan surface with no systematic lateral offsets between the upstream gullies and downstream gullies that could be due to the fault. In addition, the pretended offset gully is currently active (Fig. 4C) and therefore not beheaded as Xu et al. (2005) argue. Along the neighboring fan to the west, the streams flow at the base of the scarp (Fig. 4C) simply following topography (slope to the SW, i.e. almost parallel to the scarp, as opposed to the Maoya fan, where the scarp is almost perpendicular to the slope direction). In addition, we did not find any clear left-lateral offsets in the morphology along the entire Maoya segment on satellite images nor in the field. We therefore conclude that only dominant normal motion occurred on this fault strand since at least the fan emplacement (~22 ka).

By performing 3D numerical thermal-kinematic inversion using the Pecube code (Braun et al., 2012) on 5 apatite fission track and 2 apatite (U–Th)/He ages from samples in the Litang fault footwall, Zhang et al. (2015) determined a long-term exhumation rate of 0.59 ± 0.03 mm/yr since 6.6 ± 0.5 Ma at the Maoya fan site. This rate is identical to the vertical rate we determined at the same location at the late Quaternary timescale: 0.6 ± 0.1 mm/yr (Fig. 9), suggesting that vertical rates may have remained constant since the fault's initiation. Matching the LTFS initiation age with the long-term horizontal offsets along the Maoya segment (~6 km) yields a long-term left-lateral slip-rate of ~0.9 mm/yr (Zhang et al., 2015) (Fig. 9). This suggests that horizontal rates may have varied with time as the current nature of the Maoya segment appears to mostly be normal.

5.3. Short-term deformation rates from GPS and seismic data

Seventeen earthquakes of Mw ≥ 5 have been recorded in the USGS catalogue since 1976 close to the LTFS. Twelve of them correspond to a cluster of events that occurred in early 1989 with their epicenters lying 25 to 50 km south of the Maoya fault, with focal mechanisms implying

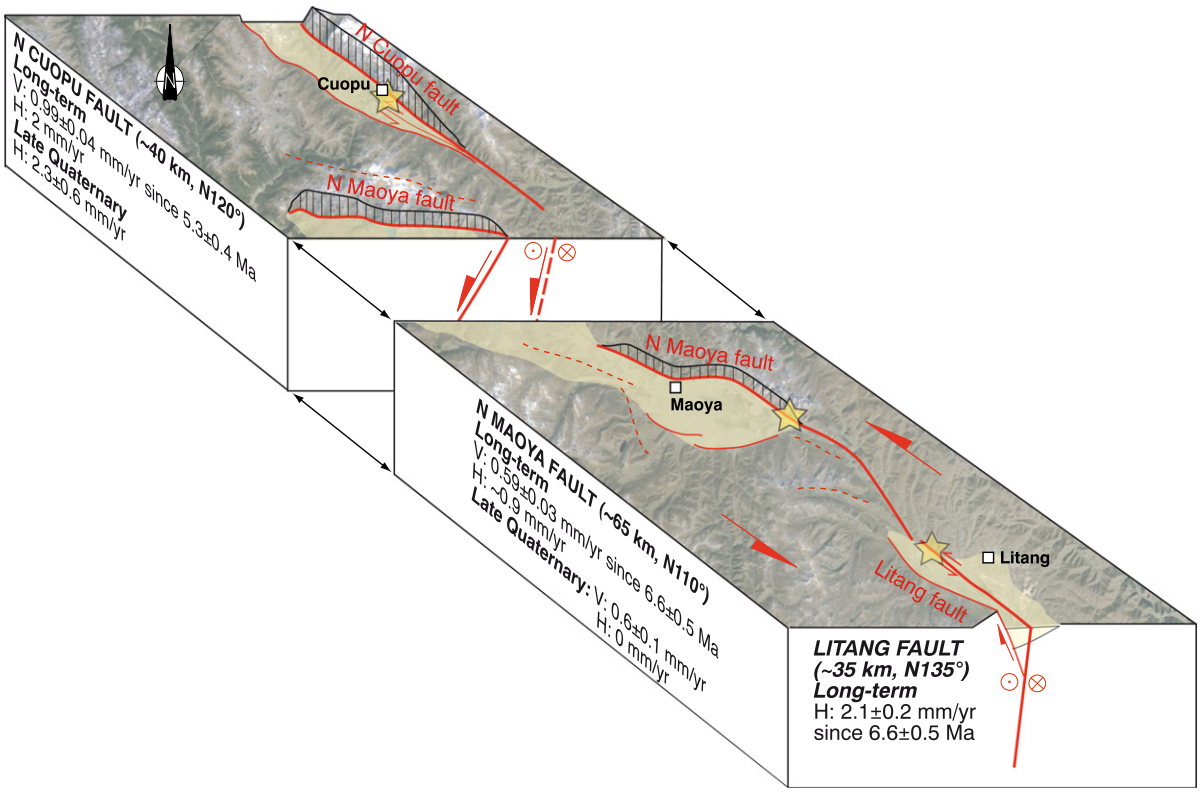

Fig. 9. 3D cartoon of the Litang fault system with Google Earth image on top. Yellow stars show locations of slip-rates determination explained in the text, which were obtained at the long-term (Zhang et al., 2015) and late Quaternary (this study) timescales. V = vertical rate, H = horizontal left-lateral slip-rate.

~EW normal faulting (Fig. 1B). One earthquake (Mw5.2, 1989/1/18) is located closer to the Litang fault, and given the uncertainties on its location (25 to 35 km difference between the CMT and the USGS catalogues), it is probable that it has occurred on that fault (Fig. 1C). Its focal mechanism shows one nodal plane trending N120° 50°S parallel to the LTFS (Fig. 1C). If this plane was the fault activated during the earthquake, motion was mostly left-lateral (pitch 15°E) with a normal component. A few months later, another earthquake (Mw6.2, 1989/5/3) occurred ~20 km south of the Maoya fault, probably rupturing its deep part since the fault dips ~50-60° toward the south. In this case, the focal mechanism shows one of the two nodal planes trending N95° 52°S parallel to the Maoya fault (Fig. 1C). If this plane was the fault activated during the earthquake, motion was mostly normal with a small left-lateral component (pitch 66°E) (Fig. 1C).

GPS data reveal a large-scale clockwise rotation of eastern Tibet relative to Eurasia around the eastern Himalayan syntaxis (Zhang et al., 2004; Gan et al., 2007; Liang et al., 2013) (Figs. 1B and S3). These velocities, derived from both campaign and permanent stations, are calculated over 3 to 15 years and are used to estimate the current slip-rate on the LTFS. While a significant 1.3 ± 0.6 to 13.1 ± 0.6 mm/yr left-lateral motion is identified across the Xianshuihe fault, the southward decrease in overall horizontal velocity across the LTFS is small given the uncertainties (1.7 ± 1.6 mm/yr), but is consistent with a 1.1 ± 0.5 mm/yr left-lateral motion along a fault trending N130° together with 2.5 ± 1.7 mm/yr of extension in the perpendicular direction (Fig. S3D,E). However, the GPS network is still too sparse and the time lag too small to yield precise slip-rate estimates, and high uncertainties remain. In addition, the data can be significantly affected by the seismic cycle. Nevertheless, at first order, GPS-derived slip-rates appear compatible with longer-term observations (~10 ka to 7 Ma) showing that the LTFS is currently left-lateral with an extensional component of a few mm/yr.

5.4. Litang fault system within SE Tibet

The fact that we and Zhang et al. (2015) determined a similar rate of ~0.6 mm/yr at ~20 ka and 5–7 Ma timescales, respectively, has important implications for the tectonics of the region. It suggests that the LTFS (or at least the Maoya segment) has been moving at a constant vertical rate of ~0.6 mm/yr since its initiation at 5–7 Ma. Using a fault's dip angle of 50° (corresponding to that of the SW dipping focal plane of the 1989/1/18 earthquake, Fig. 1C) yields an extension rate perpendicular to the fault of ~0.5 mm/yr. This amount is of the same order but slightly lower than the GPS estimates (2.5 ± 1.7 mm/yr) (see Fig. S3).

While the Cuopu and Maoya segments appear to be mostly normal since at least ~20 ka, they were most likely left-lateral strike-slip in the past (with cumulative offsets of 11–6 km, Zhang et al., 2015). Along the Litang and South Jawa-Dewu segments however, it appears that while co-seismic surface ruptures show both left-lateral and vertical offsets, cumulative horizontal offsets are harder to find. This led Zhang et al. (2015) to suggest that normal and left-lateral motions were coeval for some segments (Litang and South Jawa-Dewu along which co-seismic surface ruptures display oblique motion), but were successive for others, as attested by fault plane striations crosscutting relationship (Jawa) or long-term cumulative horizontal offsets vs short-term vertical offsets (Cuopu and Maoya). More importantly, they suggested that the Cuopu, Maoya and South Jawa faults trending ~N110–120° show an en-echelon pattern and act as releasing bends of the left-lateral Litang and Dewu segments trending ~N135°. This implies that the area is not the site of pure ~NS extension as previously assumed on the basis of few focal mechanisms (e.g., Copley, 2008) but rather of NW–SE left-lateral transtention along the LTFS.

The fact that the long-term left-lateral offsets across the LTFS are much smaller (<15 km, e.g., Zhang et al., 2015) than that across the nearby Ganzi–Yushu–Xianshuihe fault system (60–80 km, e.g.,

Burchfiel et al., 1995; Yan and Lin, 2015), suggests a younger initiation age for the former or a much slower rate, therefore possibly explaining its discontinuity compared to the very linear traces of the Ganzi–Yushu–Xianshuihe or Red River fault systems. Indeed, the 5–7 Ma (Zhang et al., 2015) initiation age of the LTFS is younger than that of the Xianshuihe fault (≥12.8 ± 1.4 Ma, e.g., Roger et al., 1995) or Red River fault (≤11 to 5 Ma for dextral slip, e.g., Leloup et al., 1993, 2001; Replumaz et al., 2001; Fyhn and Phach, 2015). This led Zhang et al. (2015) to suggest that the onset of the LTFS results from a kinematic reorganization in SE Tibet, and that it acts as a link between the two major fault systems in eastern Tibet, the Xianshuihe and the Red River fault systems (Fig. 1B), ensuring kinematic compatibility between them.

5.5. Earthquake hazard in the Litang area

The devastating 2008 Mw7.9 Wenchuan earthquake occurred in the Longmen Shan, along the eastern topographic step between the seismically active Tibetan Plateau and the tectonically stable plains of eastern China (Fig. 1A). Because more than one third of all historical M > 7 earthquakes in continental China have occurred in that transition zone (e.g., Deng et al., 2003; Zhang, 2013), it is referred to as the "NS seismic belt" (green box in Fig. 1A). We suggest however that this zoning is encompassing active faults of various kinematics and orientation and is thus not adequately depicting the seismic risk of the region. The left-lateral strike-slip Xianshuihe fault system is one of the most active faults on the Tibetan Plateau with 9 events of M > 7 since 1700 (e.g., Allen et al., 1991). This fault system is composed of 4 segments of >300 km-long, with a clear continuity and a dominant strike-slip motion (Fig. 1A,B), and could generate earthquakes of large magnitude (Allen et al., 1991), comparable to that of the Wenchuan earthquake. The LTFS is also quite active with three historical earthquakes of 7.5 > M > 7 since 1700, which if occurring today, would produce considerable damage in the Litang county, where >70,000 people live. The ~N135° trending Litang and Dewu faults have a sinistral/normal motion, as attested by the 1989/1/18 Mw5.2 earthquake focal mechanism (Fig. 1C) and the geological offsets. In 1989, rupture on this strike-slip branch has preceded by four months a larger earthquake swarm on the Maoya normal fault (16 earthquakes with 5 < Mw < 6.4 in four months), strongly suggesting interaction of the two faults. However, the LTFS appears highly segmented (Figs. 1C and 9) and it seems that most ruptures will remain restricted to individual segments, the length of these segments (35 to 60 km) supporting earthquakes of magnitudes less than Mw7.5. It is however not impossible that an event initiated on one segment could propagate to another one, inducing a larger magnitude event. The high segmentation, the low slip-rates and the current dominant normal component of motion on several segments all indicate that seismic hazard along the LTFS is smaller than along the nearby large strike-slip Xianshuihe fault system or Longmen Shan thrust belt.

6. Conclusion

We studied horizontally offset moraine crests from the Cuopu basin and a vertically offset fan from the eastern Maoya basin to determine late Quaternary slip-rates along the Litang fault system (LTFS) located in the eastern Tibetan Plateau. At Cuopu, only the oldest moraine crests are offset by the slowly slipping main secondary strike-slip fault within the Cuopu basin (the fault does not cross the youngest crests), along which we determined a very small (~0.1 mm/yr) left-lateral slip-rate. The main active N Cuopu fault is currently almost purely normal, but shows a left-lateral rate of 2.3 ± 0.6 mm/yr since 173 ka from the offset of the same moraines, in agreement with the rate of 2.1 ± 0.2 mm/yr proposed by Zhang et al. (2015) since ~5.3 Ma. The Maoya fan is vertically offset by the currently dominantly normal N Maoya fault, along which we determined a vertical rate of 0.6 ± 0.1 mm/yr since ~22 ka, which is in agreement with the exhumation rate obtained by Zhang et al. (2015) on the long-term (5–7 Ma) at the same location (0.59 ± 0.03 mm/yr). These rates at ka and Ma timescales translate into an extension rate which is slightly lower than that determined by GPS: 2.5 ± 1.7 mm/yr. Left-lateral rates along the main faults of the LTFS range between 0.9 and 2.3 mm/yr at all timescales. We confirm that at present, the Cuopu, Maoya and South Jawa segments of the LTFS are normal with a slight left-lateral component, while the Litang and Dewu segments are dominantly left-lateral with a normal component. This implies that the area is not experiencing pure ~NS extension but rather of NW–SE left-lateral transtension along the LTFS. We suggest that the slow rate, the partly normal kinematics along the LTFS, and its highly segmented geometry favor the occurrence of large earthquakes (6.5 < M <7.5) rather than of very large ones (M > 7.5), similar to those occurring along the Xianshuihe and Longmen Shan fault systems. However, the exceptional occurrence of a very large earthquake rupturing the whole Litang fault system cannot be completely ruled out.

Acknowledgments

This project was conducted under the auspices of the National Natural Science Foundation of China (NSFC 41272236, 41330211), the China Geological Survey (DD20160022-03), the Basic Outlay of Scientific Research Work from the Institute of Geology, CAGS (J1334, J1520, YYWF201601), as well as the Cai Yuanpei program (27968UC) of the China Scholarship Council/French Ministry of Education. We thank E. Kali and J. Van der Woerd from the University of Strasbourg/CNRS UMR7516 for the AMS measurements that were performed at the ASTER AMS French national facility (CEREGE, Aix-en-Provence), which is supported by the INSU/CNRS, the French Ministry of Research and Higher Education, IRD, and CEA. Part of the field-work was sponsored by the CaiYuanPei (French Foreign affairs) and SYSTER-2014 (Institut National des Sciences de l'Univers du CNRS) programs. This work has also benefited from the help in the field from Chan Wu, Wei-Kuo Lin, Yuanze Zhang, Kun Yun, Yuan Tang and Shuai Han. Special thanks to Editor Philippe Agard, as well as to Philippe Vernant and an anonymous reviewer for helpful and constructive comments.

Appendix A. Supplementary data

Supplementary data to this article can be found online at http://dx.doi.org/10.1016/j.tecto.2016.05.039.

References

Allen, C.R., Luo, Z., Qian, H., Wen, X., Zhou, H., Huang, W., 1991. Field study of a highly active fault zone: the XSF of southwestern China. Geol. Soc. Am. Bull. 103, 1178–1199.

Applegate, P.J., Urban, N.M., Laabs, B.J.C., Keller, K., Alley, R.B., 2010. Modeling the statistical distributions of cosmogenic exposure dates from moraines. Geosci. Model Dev. 3, 293–307.

Balco, G., Stone, J.O., Lifton, N.A., Dunai, T.J., 2008. A complete and easily accessible means of calculating surface exposure ages or erosion rates from ^{10}Be and ^{26}Al measurements. Quat. Geochronol. 3, 174–195. http://dx.doi.org/10.1016/j.quageo.2007.12.001.

Benedetti, L., Van der Woerd, J., 2014. Cosmogenic nuclide dating of earthquakes, faults, and toppled blocks. Elements 10 (5), 357–361.

Braun, J., van der Beek, P., Valla, P., Robert, X., Herman, F., Glotzbach, C., Pedersen, V., Perry, C., Simon-Labric, T., Prigent, C., 2012. Quantifying rates of landscape evolution and tectonic processes by thermochronology and numerical modeling of crustal heat transport using PECUBE. Tectonophysics 524–525, 1–28.

Briner, J.P., Kaufman, D.S., Manley, W.F., Finkel, R.C., 2005. Cosmogenic exposure dating of late Pleistocene moraine stabilization in Alaska. Geol. Soc. Am. Bull. 117, 1108–1120. http://dx.doi.org/10.1130/B25649.1.

Burchfiel, B.C., Chen, Z., Liu, Y., Royden, L.H., 1995. Tectonics of the Longmen Shan and adjacent regions, central China. Int. Geol. Rev. 37, 661–735.

Bureau of Geology and Mineral Resources (BGMR), 1991. Regional Geology of Sichuan Province, Geological House, Beijing.

Chevalier, M.-L., Hilley, G., Tapponnier, P., Van Der Woerd, J., Liu-Zeng, J., Finkel, R.C., Ryerson, F.J., Li, H., Liu, X., 2011. Constraints on the late Quaternary glaciations in Tibet from cosmogenic exposure ages of moraine surfaces. Quat. Sci. Rev. 30, 528–554. http://dx.doi.org/10.1016/j.quascirev.2010.11.005.

Chevalier, M.-L., Ryerson, F.J., Tapponnier, P., Finkel, R.C., Van Der Woerd, J., Haibing, L., Qing, L., 2005. Slip-rate measurements on the Karakorum fault may imply secular variations in fault motion. Science 307, 411–414. http://dx.doi.org/10.1126/science.1105466.

Chevalier, M.-L., Van der Woerd, J., Tapponnier, P., Li, H., Ryerson, F.J., Finkel, R.C., 2015. Late Quaternary slip-rate along the central Bangong segment of the Karakorum fault, western Tibet. Geol. Soc. Am. Bull. http://dx.doi.org/10.1130/B31269.1.

Clark, M.K., Royden, L.H., 2000. Topographic ooze: building the eastern margin of Tibet by lower crustal flow. Geology 28 (8), 703–706.

Copley, A., 2008. Kinematics and dynamics of the southeastern margin of the Tibetan Plateau. Geophys. J. Int. 174 (3), 1081–1100. http://dx.doi.org/10.1111/j.1365-246X.2008.03853.x.

Deng, Q., Zhang, P., Ran, Y., Yang, X., Min, W., Chu, Q., 2003. Basic characteristics of active tectonics of China. Sci. China Ser. D Earth Sci. 46, 356–372. http://dx.doi.org/10.1360/03yd9032.

Desilets, D., Zreda, M., 2003. Spatial and temporal distribution of secondary cosmic-ray nucleon intensities and applications to in-situ cosmogenic dating. Earth Planet. Sci. Lett. 206, 21–42. http://dx.doi.org/10.1016/S0012-821X(02)01088-9.

Desilets, D., Zreda, M., Prabu, T., 2006. Extended scaling factors for in situ cosmogenic nuclides: new measurements at low latitude. Earth Planet. Sci. Lett. 246, 265–276. http://dx.doi.org/10.1016/j.epsl.2006.03.051.

Dunai, T.J., 2000. Scaling factors for production rates of in situ produced cosmogenic nuclides: a critical reevaluation. Earth Planet. Sci. Lett. 176, 157–169. http://dx.doi.org/10.1016/S0012821X(99)00310-6.

Dunai, T.J., 2001. Influence of secular variation of the geomagnetic field on the production rates of in situ produced cosmogenic nuclides. Earth Planet. Sci. Lett 193, 197–212.

Fu, P., Stroeven, A.P., Harbor, J.M., Hattestrand, C., Heyman, J., Caffee, M.W., Zhou, L., 2013. Paleoglaciation of Shaluli Shan, southeastern Tibetan Plateau. Quat. Sci. Rev. 64, 121–135. http://dx.doi.org/10.1016/j.quascirev.2012.12.009.

Fyhn, M.B.W., Phach, P.V., 2015. Late Neogene structural inversion around the northern Gulf of Tonkin, Vietnam: effects from right-lateral displacement across the Red River fault zone. Tectonics 34, 290–312. http://dx.doi.org/10.1002/2014TC003674.

Gan, W., Zhang, P., Shen, Z., Niu, Z., Wang, M., Wan, Y., Zhou, D., Cheng, J., 2007. Present-day crustal motion within the Tibetan Plateau inferred from GPS measurements. J. Geophys. Res. 112, B08416. http://dx.doi.org/10.1029/2005JB004120.

Hallet, B., Putkonen, J., 1994. Surface dating of dynamic landforms: young boulders on aging moraines. Science 265, 937–940.

Hetzel, R., Niedermann, S., Tao, M.X., Kubik, P.W., Ivy-Ochs, S., Gao, B., Strecker, M.R., 2002. Low slip rates and long-term preservation of geomorphic features in Central Asia. Nature 417, 428–432.

Heyman, J., Stroeven, A.P., Harbor, J., Caffee, M.W., 2011. Too young or too old: evaluating cosmogenic exposure dating based on an analysis of compiled boulder exposure ages. Earth Planet. Sci. Lett. 302, 71–80. http://dx.doi.org/10.1016/j.epsl.2010.11.040.

Imbrie, J., Hays, J.D., Martinson, D.G., McIntyre, A., Mix, A.C., Morley, J.J., Pisias, N.G., Prell, W.L., Shackleton, N.J., 1984. The Orbital Theory of Pleistocene Climate: Support From a Revised Chronology of the Marine $\delta^{18}O$ Record. Milankovitch and Climate: Understanding the Response to Astronomical Forcing. pp. 269–305 (A. Berger, J. Imbrie, J. Hays, G. Kukla, and B. Saltzman, Reidel, Boston).

Lal, D., 1991. Cosmic-ray labeling of erosion surfaces-In situ nuclide production rates and erosion models. Earth Planet. Sci. Lett. 104 (2-4), 424–439. http://dx.doi.org/10.1016/0012-821X(91)90220-C.

Leloup, P.H., Arnaud, N., Lacassin, R., Kienast, J.R., Harrison, T.M., Trong, T.T.P., Replumaz, A., Tapponnier, P., 2001. New constraints on the structure, thermochronology, and timing of the Ailao Shan-Red River shear zone, SE Asia. J. Geophys. Res. 106 (B4), 6683–6732. http://dx.doi.org/10.1029/2000JB900322.

Leloup, P.H., Harrison, T.M., Ryerson, F.J., Chen, W., Li, Q., Tapponnier, P., Lacassin, R., 1993. Structural, petrological and thermal evolution of a tertiary ductile strike-slip shear zone, Diancang Shan, Yunnan. J. Geophys. Res. 98 (B4), 6175–6743.

Liang, S., Gan, W., Shen, C., Xiao, G., Liu, J., Chen, W., Ding, X., Zhou, D., 2013. Three-dimensional velocity field of present-day crustal motion of the Tibetan Plateau derived from GPS measurements. J. Geophys. Res. 118 (10) (2013JB010503).

Lifton, N., Bieber, J., Clem, J., Duldig, M., Evenson, P., Humble, J., Pyle, R., 2005. Addressing solar modulation and long-term uncertainties in scaling secondary cosmic rays for in situ cosmogenic nuclide applications. Earth Planet. Sci. Lett. 239, 140–161. http://dx.doi.org/10.1016/j.epsl.2005.07.001.

Liu-Zeng, J., Tapponnier, P., Gaudemer, Y., Ding, L., 2008. Quantifying landscape differences across the Tibetan Plateau: implications for topographic relief evolution. J. Geophys. Res. 113, F04018. http://dx.doi.org/10.1029/2007JF000897.

Meade, B.J., 2007. Present-day kinematics at the India–Asia collision zone. Geology 35, 81–84. http://dx.doi.org/10.1130/G22924A.1.

Owen, L.A., Caffee, M.W., Finkel, R.C., Seong, Y.B., 2008. Quaternary glaciation of the Himalayan Tibetan orogen. J. Quat. Sci. 23. http://dx.doi.org/10.1002/jqs.1203 (513-531, ISSN0267-8179).

Putkonen, J., Swanson, T., 2003. Accuracy of cosmogenic ages for moraines. Quat. Res. 59, 255–261. http://dx.doi.org/10.1016/S0033-5894(03)00006-1.

Replumaz, A., Lacassin, R., Tapponnier, P., Leloup, P.H., 2001. Large river offsets and Plio-Quaternary dextral slip rate on the Red River fault (Yunnan, China). J. Geophys. Res. 106, 819–836.

Roger, F., Calassou, S., Lancelot, J., Malavieille, J., Mattauer, M., Xu, Z., Hao, Z., Hou, L., 1995. Miocene emplacement and deformation of the Kongga-shan granite (Xianshui-he fault zone, West Sichuan, China) — geodynamic implications. Earth Planet. Sci. Lett. 130 (1-4), 201–216.

Schafer, J.M., Tschudi, S., Zhao, Z., Wu, X., Ivy-Ochs, S., Wieler, R., Baur, H., Kubik, P.W., Schluchter, C., 2002. The limited influence of glaciations in Tibet on global climate over the past 170,000 yr. Earth Planet. Sci. Lett. 194, 287–297.

Schoenbohm, L.M., Burchfiel, B.C., Liangzhong, C., Jiyun, Y., 2006. Miocene to present activity along the Red River fault, China, in the context of continental extrusion, upper-crustal rotation, and lower-crustal flow. Geol. Soc. Am. Bull. 118 (5–6), 672–688. http://dx.doi.org/10.1130/B25816.1.

Stone, J.O., 2000. Air pressure and cosmogenic isotope production. J. Geophys. Res. 105 (B10), 23,753–23,759. http://dx.doi.org/10.1029/2000JB900181.

Tapponnier, P., Xu, Z., Roger, F., Meyer, B., Arnaud, N., Wittlinger, G., Yang, J., 2001. Oblique stepwise rise and growth of the Tibet plateau. Science 294 (5547), 1671–1677.

Thatcher, W., 2007. Microplate model for the present-day deformation of Tibet. J. Geophys. Res. 112, B01401. http://dx.doi.org/10.1029/2005JB004244.

Van der Woerd, J., Ryerson, F.J., Tapponnier, P., Gaudemer, Y., Finkel, R., Meriaux, A.S., Caffee, M., Guoguang, Z., Qunlu, H., 1998. Holocene left slip-rate determined by cosmogenic surface dating on the Xidatan segment of the Kunlun fault (Qinghai, China). Geology 26, 695–698.

Xu, J., 1979. Earthquake geology in the Litang strong earthquake region, Sichuan Province. Compiling of Surveying of Earthquake Geology in Sichuan-Yunnan Strong Earthquake Region (ed. Research Team of Seismic Intensity in Southwest China). Seismological Press, Beijing, pp. 85–91 (in Chinese).

Xu, L., Zhou, S., 2009. Quaternary glaciations recorded by glacial and fluvial landforms in the Shaluli Mountains, southeastern Tibetan Plateau. Geomorphology 103, 268–275. http://dx.doi.org/10.1016/j.geomorph.2008.04.015.

Xu, X., Wen, X., Yu, G., Zheng, R., Luo, H., Zheng, B., 2005. Average slip rate, earthquake rupturing segmentation and recurrence behavior on the Litang fault zone, western Sichuan Province, China. Sci. China Ser. D 48 (8), 1183–1196. http://dx.doi.org/10.1360/04yd0072.

Yan, B., Lin, A., 2015. Systematic deflection and offset of the Yangtze River drainage system along the strike-slip Ganzi–Yushu–Xianshuihe fault zone. Tibetan Plateau: J. Geodyn. 87, 13–25. http://dx.doi.org/10.1016/j.jog.2015.03.002.

Zechar, J.D., Frankel, K.L., 2009. Incorporating and reporting uncertainties in fault slip rates. J. Geophys. Res. 114, B12407. http://dx.doi.org/10.1029/2009JB006325.

Zhang, P., 2013. A review on active tectonics and deep crustal processes of the Western Sichuan region, eastern margin of the Tibetan Plateau. Tectonophysics 584, 7–22. http://dx.doi.org/10.1016/j.tecto.2012.02.021.

Zhang, Y., Replumaz, A., Wang, G., Leloup, P.H., Gautheron, C., Bernet, M., van der Beek, P., Paquette, J.L., Wang, A., Zhang, K., Chevalier, M.L., Li, H., 2015. Timing and rate of exhumation along the Litang fault system, implication for fault re-organisation in South East Tibet. Tectonics 34. http://dx.doi.org/10.1002/2014TC003671.

Zhang, P., Shen, Z., Wang, M., Gan, W., Bürgmann, R., Molnar, P., Wang, Q., Niu, Z., Sun, J., Wu, J., 2004. Continuous deformation of the Tibetan Plateau from global positioning system data. Geology 32 (9), 809–812. http://dx.doi.org/10.1130/G20554.1.

Zhou, C., Wu, Z., Zhang, K., Li, J., Jiang, Y., Tian, T., Liu, Y., Huang, X., 2015. New chronological constraint on the co-seismic surface ruptutre segments associated with the Litang fault. Seismol. Geol. 37, 455–467. http://dx.doi.org/10.3969/j.issn.0253-4967.2015.02.009 (in Chinese).